

Chapter 6

Coherent atom-molecule oscillations

In this chapter we discuss the experimental observation of atom-molecule coherence in a Bose-Einstein condensate [64, 75], and its theoretical description in terms of the mean-field theory derived in the previous chapter. In the first section we discuss the experimental results. In the next section we calculate the magnetic-field dependence of the frequency of the coherent atom-molecule oscillations in linear-response theory. In the final section we present the results of calculations that go beyond this linear approximation.

6.1 Experiments

In the experiments of Donley *et al.* [64] and Claussen *et al.* [75], performed both in Wieman's group at JILA, one makes use of the Feshbach resonance at $B_0 = 155.041(18)$ G(auss) in the $|f = 2; m_f = -2\rangle$ hyperfine state of ^{85}Rb . The width of this resonance is equal to $\Delta B = 11.0(4)$ G and the off-resonant background scattering length is given by $a_{\text{bg}} = -443a_0$, with a_0 the Bohr radius. The difference in the magnetic moment between the open channel and the closed channel is given by $\Delta\mu = -2.23\mu_B$, with μ_B the Bohr magneton [74].

In both experiments, one starts from a stable and essentially pure condensate of about $N_c = 10000$ atoms at a magnetic field such that the effective scattering length is close to zero. This implies that, since the condensate is in the noninteracting limit, its density profile is determined by the harmonic-oscillator groundstate wave function. The harmonic external trapping potential is axially symmetric, with trapping frequencies $\nu_r = 17.4$ Hz and $\nu_z = 6.8$ Hz in the radial and axial direction, respectively.

Starting from this situation, one quickly ramps the magnetic field to a value B_{hold}

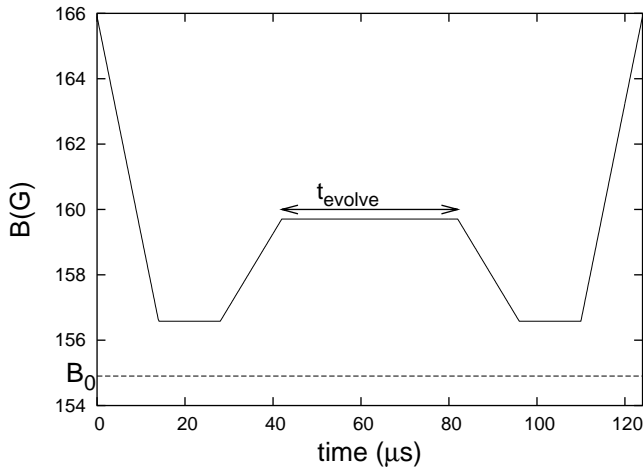


Figure 6.1: Typical magnetic-field pulse sequence as used in the experiments of Donley *et al.* [64] and Claussen *et al.* [75].

close to the resonant value and keeps it there for a short time t_{hold} before ramping to a value B_{evolve} . The magnetic field is kept at this last value for a time t_{evolve} before performing a similar pulse to go back to the initial situation. The duration of all four magnetic-field ramps is given by t_{ramp} . A typical pulse is illustrated in Fig. 6.1. Both the ramp time t_{ramp} and the hold time t_{hold} are kept fixed at values of 10–15 μs . The time t_{evolve} between the pulses is variable.

Such a double-pulse experiment is generally called a Ramsey experiment. Its significance is most easily understood from a simple system of two coupled harmonic oscillators. Consider therefore the hamiltonian

$$\hat{H} = \frac{1}{2} \begin{pmatrix} \hat{a}^\dagger & \hat{b}^\dagger \end{pmatrix} \cdot \begin{pmatrix} \delta(t) & \Delta \\ \Delta & -\delta(t) \end{pmatrix} \cdot \begin{pmatrix} \hat{a} \\ \hat{b} \end{pmatrix}, \quad (6.1)$$

where \hat{a}^\dagger and \hat{b}^\dagger create a quantum in the oscillators a and b , respectively, and Δ denotes the coupling between the two oscillators.

We consider first the situation that the detuning $\delta(t)$ is time independent. The exact solution is found easily by diagonalizing the hamiltonian. We assume that initially there are only quanta in oscillator a and none in b , so that we have that $\langle \hat{b}^\dagger \hat{b} \rangle(0) = 0$. The number of quanta in oscillator a as a function of time is then given by

$$\langle \hat{a}^\dagger \hat{a} \rangle(t) = \left[1 - \frac{\Delta^2}{(\hbar\varpi)^2} \sin^2(\varpi t/2) \right] \langle \hat{a}^\dagger \hat{a} \rangle(0), \quad (6.2)$$

with the frequency ϖ given by

$$\hbar\varpi = \sqrt{\delta^2 + \Delta^2}. \quad (6.3)$$

We see that the number of quanta in the oscillator a oscillates in time with frequency ϖ . Such oscillations are called Rabi oscillations. Note that the number of quanta in oscillator b is determined by

$$\langle \hat{b}^\dagger \hat{b} \rangle(t) = -\frac{\Delta^2}{(\hbar\varpi)^2} \sin^2(\varpi t/2) \langle \hat{a}^\dagger \hat{a} \rangle(0), \quad (6.4)$$

so that the total number of quanta is indeed conserved.

Suppose now that we start from the situation with all quanta in the oscillator a and none in b and that the detuning is such that $\delta(t) \gg \Delta$. Then we have from Eq. (6.2) that $\langle \hat{a}^\dagger \hat{a} \rangle(t) \simeq \langle \hat{a}^\dagger \hat{a} \rangle(0)$ and $\langle \hat{b}^\dagger \hat{b} \rangle(t) \simeq 0$. Starting from this situation, we change the detuning instantaneously to a value $\delta(t) \simeq 0$ and keep it at this value for a time t_{hold} . During this hold time quanta in oscillator a will go to oscillator b . Moreover, if t_{hold} is such that

$$t_{\text{hold}} \simeq \frac{\pi \hbar}{2 \Delta}, \quad (6.5)$$

on average half of the quanta in oscillator a will go to oscillator b . Such a pulse is called a $\pi/2$ -pulse. The defining property of a $\pi/2$ -pulse is that it creates a superposition of the oscillators a and b , such that the probabilities to be in oscillators a and b are equal, and therefore equal to $1/2$. This is indicated by the average $\langle \hat{a}^\dagger \hat{b} \rangle(t)$. At $t = 0$ this average is equal to zero because there is no superposition at that time. We can show that after the above $\pi/2$ -pulse the average $\langle \hat{a}^\dagger \hat{b} \rangle(t)$ reaches its maximum value. In detail, the state after the $\pi/2$ -pulse is equal to

$$\frac{1}{\sqrt{N!}} \left[\frac{\hat{a}^\dagger + \hat{b}^\dagger}{\sqrt{2}} \right]^N |0\rangle, \quad (6.6)$$

where the ground state is denoted by $|0\rangle$, and $N = \langle \hat{a}^\dagger \hat{a} \rangle(0)$.

We can now imagine the following experiment. Starting from the situation $\delta(t) \gg \Delta$, we perform a $\pi/2$ -pulse. Then jump to a certain value δ_{evolve} for a time t_{evolve} , and after this perform another $\pi/2$ -pulse and jump back to the initial situation. The number of quanta in the oscillator a , a measurable quantity, then oscillates as a function of t_{evolve} with the oscillation frequency determined by Eq. (6.3) evaluated at the detuning δ_{evolve} . The second $\pi/2$ -pulse enhances the contrast of the measurement thus providing a method of measuring the frequency ϖ as a function of the detuning with high precision.

This is basically the idea of the Ramsey experiments performed by Donley *et al.* [64] and Claussen *et al.* [75]. Roughly speaking, the atomic condensate corresponds to oscillator a and the molecular condensate to oscillator b . Therefore,

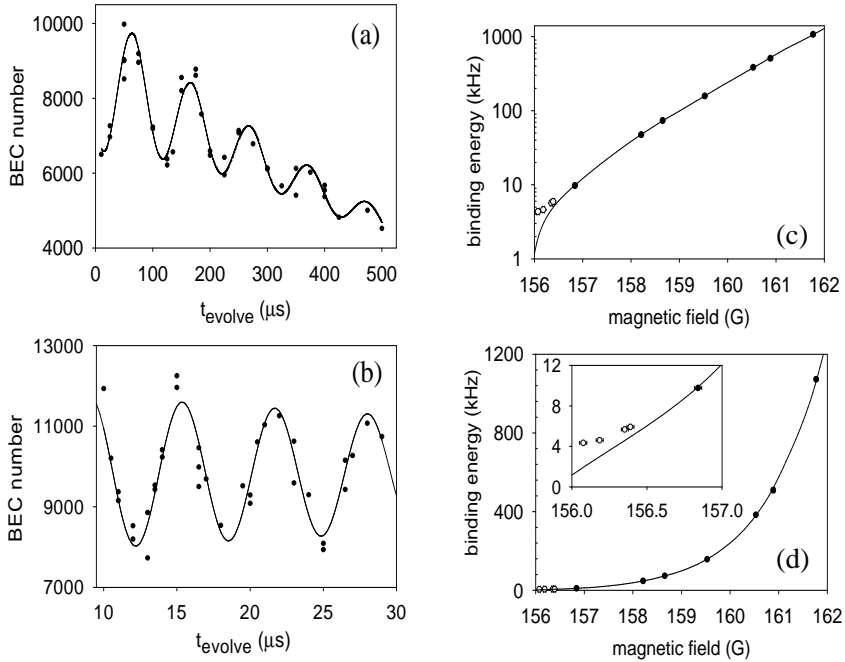


Figure 6.2: Experimental observation of coherent atom-molecule oscillations. The figures are taken from Ref. [75]. Figures (a) and (b) show the number of atoms in the atomic condensate as a function of the time between the two pulses in the magnetic field. The solid line indicates the fit in Eq. (6.7). For (a) we have that $B_{\text{evolve}} = 156.840(25)$ G. The frequency and damping rates are respectively given by $\nu_e = 2\pi \times 0.58(12)$ kHz, $\alpha = 7.9(4)$ atom/ μs , and $\beta = 2\pi \times 0.58(12)$ kHz. For (b) the magnetic field $B_{\text{evolve}} = 159.527(19)$ G and $\nu_e = 157.8(17)$ kHz. The damping is negligible for the time that is used to determine the frequency. Note that the frequency has increased for the magnetic field further from resonance. Figures (c) and (d) show the observed frequency of the coherent atom-molecule oscillations as a function of the magnetic field. The solid line is the result for the molecular binding energy found from a two-body coupled-channels calculation using the experimental results for the frequency to accurately determine the interatomic potential [75]. Only the black points were included in the fit. The inset shows that, close to resonance, the observed frequency deviates from the two-body result.

after performing the double-pulse sequence in the magnetic field one makes a light-absorption image of the atomic density from which one extracts the number of condensate and noncondensed atoms. Since this imaging technique is sensitive to a specific absorption line of the atoms it does not measure the number of molecules.

From the above discussion we expect to observe oscillations in the number of condensate atoms. Moreover, if the situation is such that the detuning between the pulses is relatively large the effect of the coupling can be neglected and the frequency of the observed oscillations corresponds to the energy difference between the atoms and the molecules, i.e., the molecular binding energy. This is indeed what is observed, thereby providing compelling evidence for the existence of coherence between atoms and molecules.

In Fig. 6.2 the experimental results of Claussen *et al.* [75] are presented. Fig. 6.2 (a) and (b) show the number of atoms in the atomic Bose-Einstein condensate as a function of t_{evolve} after a double-pulse sequence. Clearly, there is an oscillation in the number of atoms in both cases. In Fig. 6.2 (a) the magnetic field between the pulses is $B_{\text{evolve}} = 156.840(25)$ G. In Fig. 6.2 (b) we have $B_{\text{evolve}} = 159.527(19)$ G which is further from resonance. This explains also the increase in frequency from (a) to (b) since further from resonance the molecular binding energy is larger.

What is also observed is that there is a damping of the oscillations and an overall loss of condensate atoms. Experimentally, the number of atoms in the condensate is fit to the formula

$$N_c(t) = N_{\text{average}} - \alpha t + A \exp(-\beta t) \sin(\omega_e t + \phi), \quad (6.7)$$

where N_{average} is the average number of condensate atoms, A and ϕ are the oscillation amplitude and phase, respectively, and β is the damping rate of the oscillations. The overall atom loss is characterized by a rate constant α . The experimentally observed frequency is equal to $\omega_e = 2\pi \sqrt{\nu_e^2 - [\beta/2\pi]^2}$. By defining the frequency of the coherent atom-molecule oscillation in this way one compensates for the effects of the damping on the frequency. For the results in Fig. 6.2 (a) we have that $\beta = 2\pi \times 0.58(12)$ kHz and $\alpha = 7.9(4)$ atom/ μ s. The frequency is equal to $\nu_e = 9.77(12)$ kHz. For Fig. 6.2 (b) the frequency is equal to $\nu_e = 157.8(17)$ kHz. The damping and loss rate are negligible for the short time used to determine the frequency. It is found experimentally that both the damping rate and the loss rate increase as B_{evolve} approaches the resonant value.

In Fig. 6.2 (c) and (d) the results for the frequency as a function of B_{evolve} are presented. The solid line shows the result of a two-body coupled-channels calculation of the molecular binding energy [75]. The parameters of the interatomic potentials are fit to the experimental results for the frequency. Clearly, the frequency of the coherent atom-molecule oscillations agrees very well with the molecular binding energy in vacuum over a large range of the magnetic field. Moreover, in the magnetic-field

range $B_{\text{evolve}} \simeq 157\text{--}159\text{ G}$ the frequency of the oscillations is very well described by the formula $|\epsilon_m(B)| = \hbar^2/ma^2(B)$ for the binding energy, derived in Section 4.1.2. Close to resonance, however, the measured frequency deviates from the two-body result. The deviating experimental points are shown by open circles and are not taken into account in the determination of the interatomic potential. This deviation is due to many-body effects [76].

Although some of the physics of these coherent atom-molecule oscillations can roughly be understood by a simple two-level picture, it is worth noting that the physics of a Feshbach resonance is much richer. First of all, during Rabi oscillations in a simple two-level system *one* quantum in a state oscillates to the other state. In the case of a Feshbach resonance *pairs* of atoms oscillate back and forth between the dressed-molecular condensate and the atomic condensate. Therefore, the hamiltonian is not quadratic in the annihilation and creation operators and the physics is more complicated. In particular the dressed molecule may decay into two noncondensed atoms instead of forming two condensate atoms. This process is discuss in detail below. Second, the observed atom-molecule oscillations are oscillations between an atomic condensate and a dressed molecular condensate. The fact that one of the levels is a dressed molecule implies that by changing the magnetic field not only the detuning is altered, but also the internal state of the molecule itself.

This is seen most easily by considering the linearized version of the time-dependent mean-field equation in Eq. (5.16). Writing $\phi_a(t) = \phi_a e^{-i\mu t/\hbar} + \delta\phi_a(t)$ and $\phi_m(t) = \phi_m e^{-2i\mu t/\hbar} + \delta\phi_m(t)$, we have that

$$\begin{aligned} i\hbar \frac{\partial \delta\phi_m(t)}{\partial t} &= \left[\delta(B) - g^2 \frac{m^{3/2}}{2\pi\hbar^3} i \sqrt{i\hbar \frac{\partial}{\partial t} - 2\hbar\Sigma^{\text{HF}}} \right] \delta\phi_m(t) + 2g\phi_a \delta\phi_a(t), \\ i\hbar \frac{\partial \delta\phi_a(t)}{\partial t} &= 2g\phi_a^* \delta\phi_m(t), \end{aligned} \quad (6.8)$$

where we neglected the off-resonant part of the interatomic interactions. This is justified sufficiently close to resonance, where we are also allowed to neglect the energy-dependence of the atom-molecule coupling constant.

Consider first the situation that the fractional derivative is absent in the linearized mean-field equations in Eq. (6.8), i.e., we are dealing with the model of Drummond *et al.* [65], and Timmermans *et al.* [66, 78]. These coupled equations describe exactly the same Rabi oscillations as the coupled harmonic oscillators in Eq. (6.1), with the coupling equal to $\Delta = |4g\phi_a|$. In the context of particle-number oscillations between condensates, Rabi oscillations are referred to as Josephson oscillations and the associated frequency is called the Josephson frequency. The Josephson frequency in the absence of the fractional derivative term in Eq. (6.8) is given by

$$\hbar\omega_J^{\text{bare}} = \sqrt{\delta^2(B) + 16g^2n_a}, \quad (6.9)$$

which reduces to $\hbar\omega_J^{\text{bare}} \simeq |\delta(B)|$ sufficiently far off resonance where the coupling may be neglected. This result does not agree with the experimental result because, by neglecting the fractional derivative, which corresponds to the molecular self-energy, we are describing Josephson oscillations between an atomic condensate and a condensate of bare molecules instead of dressed molecules. Furthermore, using the result in Eq. (6.2) we have that the amplitude of these oscillations is given by

$$A_J^{\text{bare}} = \frac{16g^2 n_a}{[\delta(B)]^2}. \quad (6.10)$$

In first approximation we take the dressing of the molecules into account as follows. If we are in the magnetic-field range where the Josephson frequency deviates not too much from the molecular binding energy, we are allowed to expand the propagator of the molecules around the pole at the bound-state energy. As we have seen in Section 4.1.3 this corresponds to introducing the dressed molecular field and leads to the Heisenberg equations of motion in Eq. (4.31). The linearized mean-field equations that describe the Josephson oscillations of a atomic and a dressed-molecular condensate are therefore given by

$$\begin{aligned} i\hbar \frac{\partial \delta\phi_m(t)}{\partial t} &= \epsilon_m(B)\delta\phi_m(t) + 2g\sqrt{Z(B)}\phi_a\delta\phi_a(t), \\ i\hbar \frac{\partial \delta\phi_a(t)}{\partial t} &= 2g\sqrt{Z(B)}\phi_a^*\delta\phi_m(t), \end{aligned} \quad (6.11)$$

and lead to the Josephson frequency

$$\hbar\omega_J = \sqrt{\epsilon_m^2(B) + 16g^2 Z(B)n_a}, \quad (6.12)$$

which reduces to $\hbar\omega_J \simeq |\epsilon_m(B)|$ in the situation where the coupling is much smaller than the binding energy. This result agrees with the experimental fact that the measured frequency is, sufficiently far from resonance, equal to the molecular binding energy. Moreover, the initial deviation from the two-body result in the measured frequency is approximately described by the equation for the Josephson frequency in Eq. (6.12). The amplitude of the oscillations is in this case given by

$$A_J = \frac{16g^2 Z(B)n_a}{[\epsilon_m(B)]^2}, \quad (6.13)$$

which close to resonance is much larger than the result in Eq. (6.10).

To get more quantitative understanding of the magnetic-field dependence of the Josephson frequency over the entire experimentally investigated range of magnetic field we calculate this frequency in a linear-response approximation, including the energy-dependence of the atom-molecule coupling and the atom-atom interactions.

Before doing so, we make some remarks about the origin of the damping of the coherent atom-molecule oscillations and the overall loss of atoms that is observed in the experiments. One contribution to the damping is expected to be due to rogue dissociation [73]. Physically, this process corresponds to a pair of condensate atoms forming a dressed condensate molecule that then breaks up into two noncondensed atoms instead of oscillating back to the atomic condensate. This process is incorporated into our theory by the imaginary part of the molecular self-energy. As explained in Section 4.1.3 in the derivation of the Heisenberg equations of motion in Eq. (4.31), that involve the dressed molecules, we have neglected such a process. It is, however, incorporated in the full solution of the mean-field equation in Eq. (5.16). In the last section of the chapter we present the results of numerical solutions of these equations.

The overall loss of atoms from the atomic condensate is also partially due to the rogue-dissociation process. The experimental fact that a significant thermal component is formed during the double-pulse sequence supports this idea. Apart from this process, it may also be that conventional loss processes, such as dipolar decay and three-body recombination play a role. Although such processes are expected to become more important near a Feshbach resonance, they are, however, not included in our simulations since there is no detailed knowledge about the precise magnetic-field dependence near the resonance. In principle, however, these loss processes could be straightforwardly included in our calculations, by adding the appropriate imaginary terms to the mean-field equations. Another possible mechanism is the loss of atoms due to elastic collisions, the so-called quantum evaporation process [41]. This process is also not included in our present calculations.

6.2 Josephson frequency

With the mean-field theory derived in the previous chapters we now calculate the magnetic-field and density dependence of the Josephson frequency of the coherent atom-molecule oscillations, in a linear approximation. The only parameter that has not been determined yet is the effective range of the interatomic interactions r_{bg} . All other parameters are known for ^{85}Rb .

The effective range is determined by calculating the molecular binding energy in vacuum and comparing the result with the experimental data. We have seen that far off resonance the Josephson frequency is essentially equal to the molecular binding energy. Since the effect of a nonzero effective range only plays a role for large energies, and thus is important far off resonance, this comparison uniquely determines the effective range. As explained in detail in Section 4.1.2, the molecular binding energy is determined by solving for E in the equation

$$E - \delta(B) - \hbar \Sigma_{\text{m}}^{(+)}(E) = 0. \quad (6.14)$$

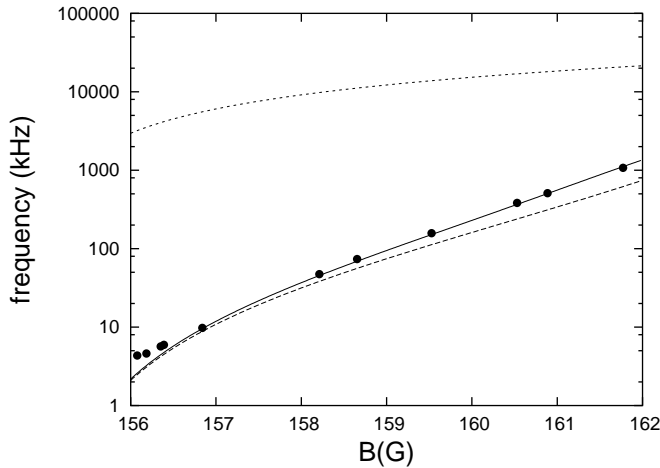


Figure 6.3: Molecular binding energy in vacuum. The solid line shows the result of a calculation with $r_{\text{bg}} = 185a_0$. The dashed line shows $|\epsilon(B)| = \hbar^2/ma^2$. The experimental points are taken from [75]. The dotted line shows the detuning $|\delta(B)|$.

For ^{85}Rb the background scattering length is negative and the effective range turns out to be positive. The retarded molecular self-energy is therefore given by

$$\hbar \Sigma_{\text{m}}^{(+)}(E) = -\frac{g^2 m}{2\pi \hbar^2 \sqrt{1 - 2\frac{r_{\text{bg}}}{a_{\text{bg}}}}} \left[\frac{i \sqrt{\left(1 - 2\frac{r_{\text{bg}}}{a_{\text{bg}}}\right) \frac{mE}{\hbar^2} - \frac{r_{\text{bg}} mE}{2\hbar^2}}}{1 + i a_{\text{bg}} \sqrt{\left(1 - 2\frac{r_{\text{bg}}}{a_{\text{bg}}}\right) \frac{mE}{\hbar^2} - \frac{r_{\text{bg}} a_{\text{bg}} mE}{2\hbar^2}}} \right]. \quad (6.15)$$

In Fig. 6.3 the result of the numerical solution of Eq. (6.14) is shown for $r_{\text{bg}} = 185a_0$. Also shown in this figure are the experimental data points. Clearly, far off resonance there is good agreement between our results and the experimental data points. Therefore, we use this value for the effective range from now on in all our calculations. The absolute value of the detuning is shown by the dotted line, and deviates significantly from the binding energy. The dashed line in Fig. 6.3 indicates the formula $|\epsilon_{\text{m}}| = \hbar^2/ma^2$. As we have derived in Section 4.1.2 this formula should accurately describe the magnetic-field dependence of the binding energy close to resonance. Clearly, the solid line that indicates the result that includes the nonzero effective range becomes closer to the dashed line as we approach resonance. However, there is a significant range of magnetic field where we need to include the effective range in our calculations. Closer to the resonance, the experimental points start to deviate from the two-atom binding energy. This deviation is taken into account by considering many-body effects.

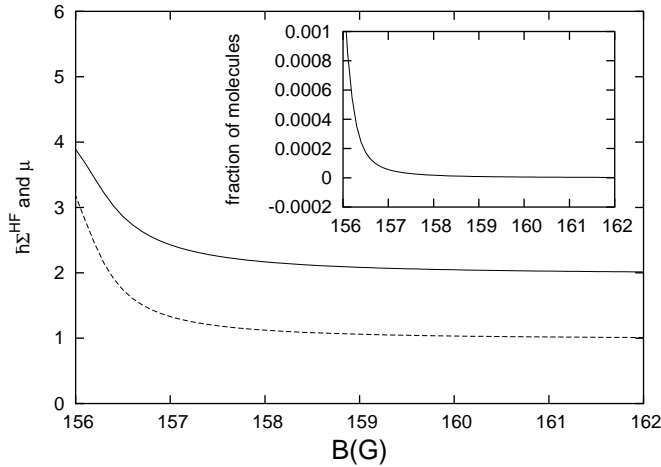


Figure 6.4: Hartree-Fock self-energy (solid line) and chemical potential (dashed line) as a function of the magnetic field for an atomic condensate density of $n_a = 2 \times 10^{12} \text{ cm}^{-3}$. Both quantities are shown in units of $4\pi a(B)\hbar^2 n_a/m$. Far off resonance, where the energy dependence of the interactions can be safely neglected we have that $\hbar \Sigma^{\text{HF}} = 8\pi a(B)\hbar^2 n_a/m$ and $\mu = 4\pi a(B)\hbar^2 n_a/m$, as expected. The inset shows the fraction of bare molecules as a function of the magnetic field.

As mentioned previously, we calculate the many-body effects on the frequency of the coherent atom-molecule oscillations in linear approximation. Therefore, we first need to determine the equilibrium around which to linearize. In detail, the equilibrium values of the atomic and molecular condensate wave functions are determined by solving the time-independent mean-field equations in Eq. (5.2) together with the equation for the Hartree-Fock self-energy in Eq. (5.3) at a fixed chemical potential μ . To compare with the experimental results it is more convenient to solve these equations at a fixed condensate density. The chemical potential is then determined from these equations.

In Fig. 6.4 we show the result of this calculation for an atomic condensate density of $n_a = 2 \times 10^{12} \text{ cm}^{-3}$. The solid line shows the Hartree-Fock self-energy $\hbar \Sigma^{\text{HF}}$ and the dashed line the chemical potential as a function of the magnetic field, both in units of the energy $4\pi a(B)\hbar^2 n_a/m$. Note that far off resonance, where the energy dependence of the interaction may be neglected, we have that $\mu = 4\pi a(B)\hbar^2 n_a/m$ and $\hbar \Sigma^{\text{HF}} = 2\mu$. This is the expected result. The inset of Fig. 6.4 shows the fraction of bare molecules $|\phi_m|^2/n_a$. Note that this fraction is always very small. This justifies neglecting the atom-molecule and molecule-molecule interactions since from this figure we see that the mean-field energies associated with these interactions are at least three orders of magnitude smaller. *A posteriori* this observation also justifies

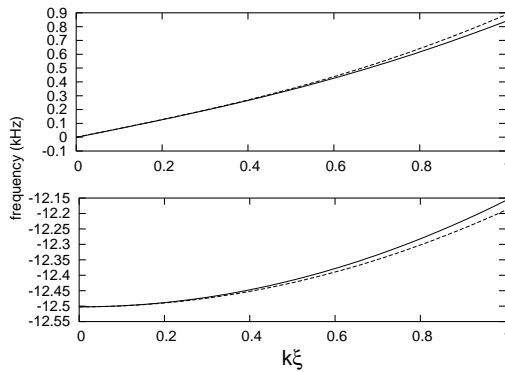


Figure 6.5: The dispersion relation for the collective modes of an atom-molecule system for a condensate density of $n_a = 2 \times 10^{12} \text{ cm}^{-3}$ at a magnetic field of $B = 157 \text{ G}$. The momentum is measured in units of the inverse coherence length $\xi^{-1} = \sqrt{16\pi a(B)n_a}$. The upper branch corresponds to the gapless dispersion for phonons. The solid line is the result of the full calculation, the dashed line shows the Bogoliubov dispersion for the scattering length $a(B)$. The lower branch corresponds to the coherent atom-molecule oscillations. The solid line is the result of the full calculation whereas the dashed line shows the result with the same zero-momentum part, but with the momentum dependence determined by $\hbar^2 \mathbf{k}^2 / 4m$.

the approach of Köhler *et al.* [79].

Since the coherent atom-molecule oscillations are a collective mode where the amplitude of the atomic and molecular condensate wave functions oscillate out-of-phase, we study the collective modes of the system. As explained in detail in the previous chapter, the frequencies of the collective modes are determined by Eq. (5.12). This equation is solved numerically and yields a dispersion relation with two branches.

The result of this calculation is shown in Fig. 6.5 for an atomic condensate density of $n_a = 2 \times 10^{12} \text{ cm}^{-3}$ and a magnetic field of $B = 157 \text{ G}$. The momentum is indicated in units of the inverse coherence length $\xi^{-1} = \sqrt{16\pi a(B)n_a}$. The upper branch corresponds to the gapless phonon excitations. For small momenta this branch has a linear momentum dependence. The upper dashed line indicates the Bogoliubov dispersion in Eq. (5.8) evaluated at the scattering length $a(B)$. For small momentum the solid and the dashed line are almost identical. For larger momenta the numerically exact result is smaller, due to the energy-dependence of the interactions that effectively reduce the scattering length.

The lower branch corresponds to the coherent atom-molecule oscillations and is gapped. The solid line indicates the result of the full calculations. For small momenta it is well described by

$$\hbar\omega_{\mathbf{k}} \simeq -\hbar\omega_J + \epsilon_{\mathbf{k}}/2, \quad (6.16)$$

where ω_J is the Josephson frequency. The dispersion resulting from this last equation

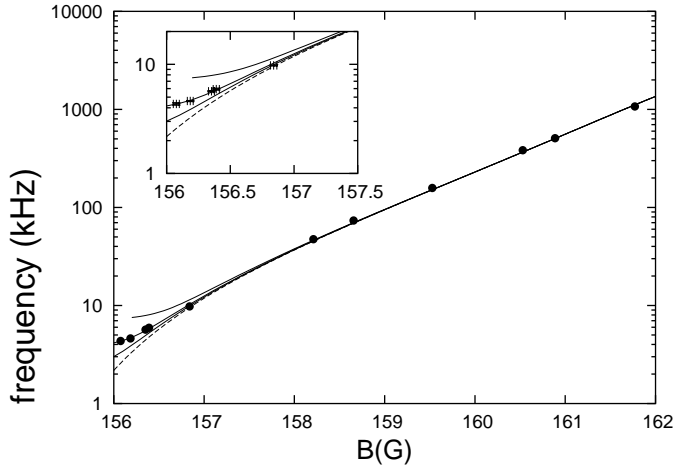


Figure 6.6: Josephson frequency of coherent atom-molecule oscillations for various values of the condensate density. The solid lines are the results of calculations for nonzero condensate density. The different lines correspond from top to bottom to the decreasing condensate densities $n_a = 5 \times 10^{12} \text{ cm}^{-3}$, $n_a = 2 \times 10^{12} \text{ cm}^{-3}$, and $n_a = 10^{12} \text{ cm}^{-3}$. The dashed line corresponds to the molecular binding energy in vacuum, i.e., $n_a = 0$. The experimental data points, taken from Ref. [75], are also shown.

is shown in the lower part Fig. 6.5 by the dashed line. This momentum dependence is to be expected since sufficiently far from resonance the atom-molecule oscillations reduce to a two-body excitation. The fact that the dispersion is negative is due to the fact that we are linearizing around a metastable situation with more atoms than molecules. Although this is the experimentally relevant situation, the true equilibrium situation for negative detuning corresponds to almost all atoms in the molecular state [78].

In Fig. 6.6 we present the results for the Josephson frequency as a function of the magnetic field, for different values of the condensate density. The solid lines in this figure show, from top to bottom, the results for an decreasing nonzero condensate density. The respective condensate densities are given by $n_a = 5 \times 10^{12} \text{ cm}^{-3}$, $n_a = 2 \times 10^{12} \text{ cm}^{-3}$, and $n_a = 10^{12} \text{ cm}^{-3}$. The dashed line shows the molecular binding energy in vacuum. The Josephson frequency reduces to the molecular binding energy for all values of the condensate density, in agreement with previous remarks. Nevertheless, sufficiently close to resonance there is a deviation from the two-body result due to many-body effects. This deviation becomes larger with increasing condensate density.

In order to confront our results with the experimental data we have to realize that the experiments are performed in a magnetic trap. Taking only the ground states

$\phi_a(\mathbf{x})$ and $\phi_m(\mathbf{x})$ into account for both the atomic and the molecular condensates, respectively, this implies effectively that the atom-molecule coupling g is reduced by an overlap integral. Hence we define the effective homogeneous condensate density by means of $n_a = N_a \left[\int d\mathbf{x} \phi_a^2(\mathbf{x}) \phi_m(\mathbf{x}) \right]^2 = 16\sqrt{2} N_a m^{3/2} v_r \sqrt{v_z} / (125\pi^3 \hbar^{3/2})$, where N_a denotes the number of condensed atoms and v_r and v_z the radial and axial trapping frequencies, respectively. For the experiments of Claussen *et al.* we have that $N_a \simeq 8000$ during the oscillations close to resonance as seen from Fig. 6.2, which results in an effective density of $n_a \simeq 2 \times 10^{12} \text{ cm}^{-3}$. This agrees also with the effective homogeneous density quoted by Claussen *et al.* [75]. The solid curve in Fig. 6.6 clearly shows an excellent agreement with the experimentally observed frequency for this density.

It is important to note that there are two hidden assumptions in the above comparison. First, we have used that the dressed molecules are trapped in the same external potential as the atoms. This is not obvious because the bare molecular state involved in the Feshbach resonance is high-field seeking and therefore not trapped. However, Eq. (4.16) shows that near resonance almost all the amplitude of the dressed molecule is in the low-field seeking open channel and its magnetic moment is therefore almost equal to twice the atomic magnetic moment. Second, we have determined the frequency of the coherent atom-molecule oscillations in equilibrium. In contrast, the observed oscillations in the number of condensate atoms is clearly a nonequilibrium phenomenon. This is, however, expected not to play an important role because the Ramsey-pulse sequence is performed on such a fast time scale that the response of the condensate wave function can be neglected. By variationally solving the Gross-Pitaevskii equation for the atomic condensate wave function, we have explicitly checked that after a typical pulse sequence its width is only a few percent larger than the harmonic oscillator ground state.

Finally, we calculate the Josephson frequency as a function of the condensate density. The results of this calculation are presented in Fig. 6.7, for various values of the magnetic field which is kept fixed in these calculations. In the presentation of the results we have subtracted the molecular binding energy to bring out the many-body effects more clearly. As expected, the difference between the Josephson frequency and the molecular binding energy increases with increasing condensate density. Moreover, for values of the magnetic field closer to resonance the difference is also larger.

The above calculations in the linear approximation give already a great deal of insight in the coherent atom-molecule oscillations, and, in particular, in their many-body aspects. In the next section we discuss the full solution of the time-dependent mean-field equations for the double-pulse experiments. We also discuss the rogue-dissociation process. The outcome of these experiments has first been discussed by Kokkelmans and Holland [74], Mackie *et al.* [73], and Köhler *et al.* [79], on the basis

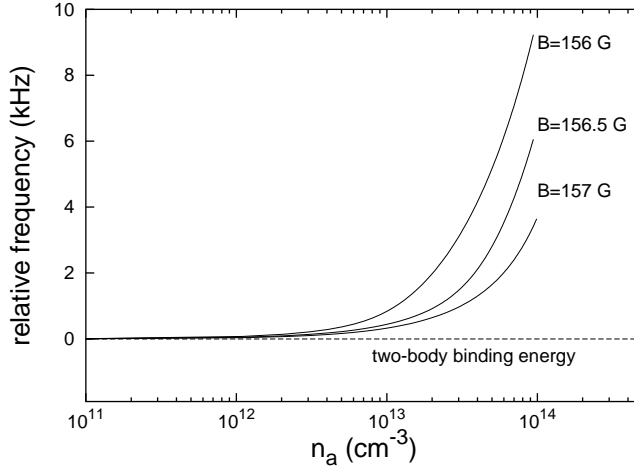


Figure 6.7: Josephson frequency of coherent atom-molecule oscillations as a function of the condensate density, for fixed magnetic field. We have subtracted the molecular binding energy.

of their mean-field approaches summarized in Section 5.2.

6.3 Beyond linear response

In this section we discuss the numerical solution of the time-dependent mean-field equations using the methods described in Sec. 5.1.2. We focus here on the situation where the detuning is only changed instantaneously, so that we are allowed to use the Green's function method discussed in this section. After the elimination of the molecular condensate wave function from the mean-field equations, the effective equation for the atomic condensate wave function is given by

$$\begin{aligned}
 i\hbar \frac{\partial \phi_a(t)}{\partial t} &= \frac{4\pi a_{bg} \hbar^2}{m} |\phi_a(t)|^2 \phi_a(t) \\
 &+ 2g\phi_a^*(t)\phi_m(0)e^{-i\epsilon_m(B)t/\hbar} - \frac{2ig^2\phi_a^*(t)}{\hbar} \int_0^t dt' \left\{ Z(B)e^{-\frac{i}{\hbar}\epsilon_m(B)(t-t')}\phi_a^2(t') \right. \\
 &\left. + \frac{g^2m^{3/2}}{\pi\hbar^2} \int_0^\infty \frac{d\omega}{2\pi} \frac{\sqrt{\hbar\omega}e^{-i(\omega+2\Sigma^{\text{HF}})(t-t')}\phi_a^2(t')}{[\hbar\omega+2\hbar\Sigma^{\text{HF}}-\delta(B)]^2 + (g^4m^3/4\pi^2\hbar^6)\hbar\omega} \right\}. \quad (6.17)
 \end{aligned}$$

In this equation, the term that involves the integral over frequencies describes the fact that a pair of condensate atoms that forms a molecule can decay into a pair of noncondensed atoms with opposite momenta, i.e., the rogue-dissociation process. In

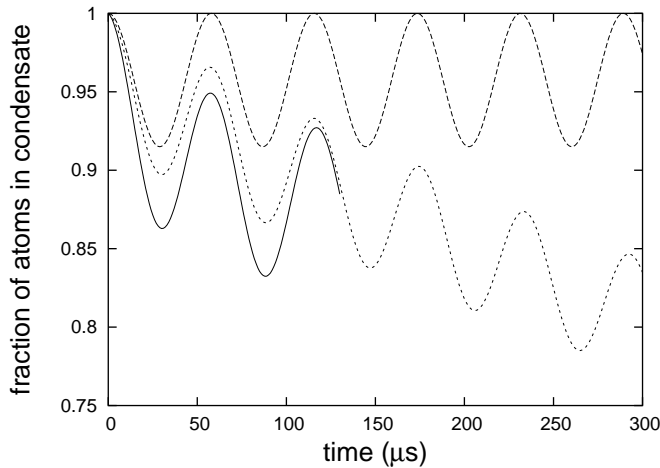


Figure 6.8: Fraction of atoms in the atomic condensate. The solid line shows the result of the inclusion of the rogue-dissociation process into the calculations. The dashed line shows the result of a calculation without this process. The dotted line shows the result for a calculation that includes the estimate in Eq. (6.21). We have taken the parameters $B_{\text{init}} = 162$ G, $B_{\text{evolve}} = 158$ G, and $n_a = 2 \times 10^{12} \text{ cm}^{-3}$.

the absence of this term the equation effectively takes into account the dressing of molecules in an adiabatic manner, and describes Josephson oscillations between a condensate of atoms and dressed molecules.

As we have discussed in the previous chapter, the above equation is only applicable to the situation of a sudden change in magnetic field. Therefore, we perform the following calculation. For a given magnetic field B_{init} and atomic condensate density we calculate the equilibrium values of the molecular wave functions and the Hartree-Fock self-energy, using the time-independent mean-field equations in Eq. (5.2) and Eq. (5.3). Then we change the magnetic field instantaneously to the value B_{evolve} and keep it at this value. In Fig. 6.8 the results of the calculations for this situation are shown, with $B_{\text{init}} = 162$ G and $B_{\text{evolve}} = 158$ G. The atomic condensate density is taken equal to $n_a = 2 \times 10^{12} \text{ cm}^{-3}$. The dashed line shows the result for a calculation without the rogue-dissociation process and shows oscillations where a fraction of the atoms is converted into molecules and oscillates back and forth between the atomic and dressed molecular condensate. Since there is no decay mechanism, all of the atoms come back into the atomic condensate at times equal to a multiple of the oscillation period. The solid line shows the result of a calculation that includes the rogue-dissociation process. Clearly, the number of condensate atoms oscillates in this case as well. However, not all of the atoms come back into the atomic condensate and there is a decay of the number of atoms in the atomic condensate. This is

precisely due to the above-mentioned rogue-dissociation process.

Although the preliminary calculations presented in this section are limited to the case of a step in the magnetic field, they nevertheless present some insight in the effects of the rogue-dissociation process on the coherent atom-molecule oscillations in a Ramsey experiment. In future work we intend to study also the case of time-dependent magnetic fields, by an exact numerical treatment of the fractional derivative in our time-dependent mean-field equations. In particular, we are interested in the magnetic-field dependence of the damping that is caused by the rogue-dissociation process.

We can estimate this dependence as follows. The Green's function associated with the rogue-dissociation process,

$$G_{\text{rog}}^{(+)}(t-t') = -\frac{i\theta(t-t')g^2m^{3/2}}{\pi\hbar^2} \times \int_0^\infty \frac{d\omega}{2\pi} \frac{\sqrt{\hbar\omega}e^{-i(\omega+2\Sigma^{\text{HF}})(t-t')}}{[\hbar\omega + 2\hbar\Sigma^{\text{HF}} - \delta(B)]^2 + (g^4m^3/4\pi^2\hbar^6)\hbar\omega}, \quad (6.18)$$

is sharply peaked in time. Hence we approximate this Green's function by

$$G_{\text{rog}}^{(+)}(t-t') \simeq \tau(B)G_{\text{rog}}^{(+)}(0)\delta(t-t'), \quad (6.19)$$

with the timescale $\tau(B)$ given by

$$\tau(B) = \int_{-\infty}^{t_c} dt G_{\text{rog}}^{(+)}(t), \quad (6.20)$$

with t_c a positive cut-off that is determined such that the result for $\tau(B)$ depends only very weakly on t_c . The Green's function evaluated at zero time $G_{\text{rog}}^{(+)}(0) = 1 - Z(B)$, a result which follows from the sum rule for the molecular density of states in Eq. (4.15). This gives the contribution

$$\simeq \frac{-2i[1 - Z(B)]g^2\tau(B)}{\hbar} |\phi_a(t)|^2 \phi_a(t), \quad (6.21)$$

to the right-hand side of Eq. (6.17). The rate equation for the atomic density that follows from this term is given by

$$\frac{dn_a}{dt} \simeq -\frac{4[1 - Z(B)]g^2\tau(B)}{\hbar^2} n_a^2(t), \quad (6.22)$$

which leads after linearization to the following equation for the number of condensate atoms

$$\frac{d\delta N_a(t)}{dt} \simeq -\beta\delta N_a(t), \quad (6.23)$$

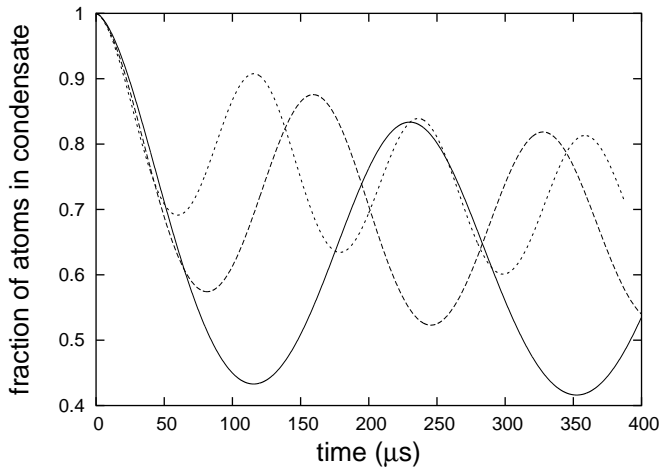


Figure 6.9: Fraction of atoms in the atomic condensate after a step in the magnetic field. The solid line corresponds to $B_{\text{evolve}} = 156.1$ G. The dashed and dotted line correspond to a magnetic field of $B_{\text{evolve}} = 156.5$ G and $B_{\text{evolve}} = 156.9$ G, respectively. The initial magnetic field is $B_{\text{nit}} = 162$ G and the density of the atomic condensate is $n_a = 2 \times 10^{12} \text{ cm}^{-3}$.

with the rate β given by

$$\beta \simeq \frac{8[1 - Z(B)]g^2\tau(B)n_a}{\hbar^2}. \quad (6.24)$$

We observe from this equation that the loss rate of atoms from the atomic condensate due to the rogue-dissociation process increases as the magnetic field approaches its resonant value. This is indeed what is observed experimentally [75]. Far off resonance the loss rate vanishes since the wave function renormalization factor $Z(B) \rightarrow 1$ in this limit. For the parameters of Fig. 6.2 (a) at the effective homogeneous density $n_a = 2 \times 10^{12} \text{ cm}^{-3}$, we have that $\tau(B) \simeq 1.28 \times 10^{-9}$ s, which leads to $\beta \simeq 0.45$ kHz. The dotted line in Fig. 6.8 shows the result of a calculation that includes the term in Eq. (6.21). The exact result, shown by the solid line, and this approximate result show the same overall damping rate. This justifies the approximation for the Green's function in Eq. (6.19). The result for the damping rate β is about a factor of eight smaller than the experimental result.

To further investigate the magnetic-field dependence of the damping of the coherent atom-molecule oscillations, we have calculated the numerical solution of the effective equation of motion for the atomic condensate wave function for a step in the magnetic field, for three different final magnetic fields. The results of these calculations are shown in Fig. 6.9. The solid, dashed, and dotted lines corresponds to magnetic field of $B_{\text{evolve}} = 156.1$ G, $B_{\text{evolve}} = 156.5$ G, and $B_{\text{evolve}} = 156.9$ G, re-

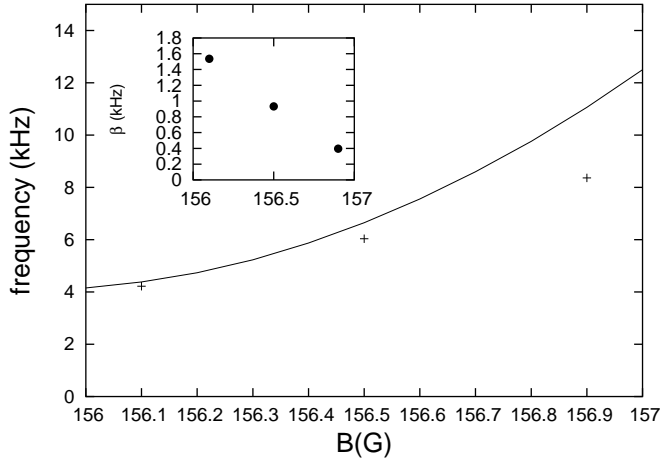


Figure 6.10: Frequency and damping as a function of the magnetic field. The solid line corresponds to the frequency found by means of linear-response theory.

spectively. The initial equilibrium corresponds to an atomic condensate density of $n_a = 2 \times 10^{12} \text{ cm}^{-3}$ at a magnetic field of $B_{\text{init}} = 162 \text{ G}$. Note the increase in the frequency with increasing magnetic field.

The magnetic-field dependence of the frequency and damping of the coherent atom-molecule oscillations is found from these numerical results by fitting with the equation in Eq. (6.7). The results are presented in Fig. 6.10. The solid line corresponds to the Josephson frequency of the coherent atom-molecule oscillations that was found by means of the linear-response calculation of the previous section. The deviation for large magnetic fields is understood because we have, in our numerical solution of the effective mean-field equation, not taken into account the higher-order energy-dependences of the molecular self-energy that are taken into account in the linear-response theory. The inset shows the damping as a function of the magnetic field. Note the increase of the damping as the magnetic field approaches its resonant value. This is expected from the estimate in Eq. (6.24).

The above analysis indicates that the rogue-dissociation process gives possibly a contribution to the experimentally observed damping of the coherent atom-molecule oscillations. Presumably, however, also other mechanisms contribute to the observed damping. In particular, we mention here the quantum evaporation process, that was shown to be important in the single-pulse experiments [41]. The detailed investigation of the damping of the coherent atom-molecule oscillation is a subject for further study.